

Scanning tunneling spectroscopy and surface quasiparticle interference in models for the strongly correlated topological insulators SmB_6 and PuB_6

Pier Paolo Baruselli and Matthias Vojta

Institut für Theoretische Physik, Technische Universität Dresden, 01062 Dresden, Germany

(Received 30 September 2014; revised manuscript received 23 October 2014; published 11 November 2014)

SmB_6 is one of the candidate compounds for topological Kondo insulators, a class of materials which combines a nontrivial topological band structure with strong electronic correlations. Here we employ a multiband tight-binding description, supplemented by a slave-particle approach to account for strong interactions, to theoretically study the surface-state signatures in scanning tunneling spectroscopy and quasiparticle interference (QPI). We discuss the spin structure of the three surface Dirac cones of SmB_6 and provide concrete predictions for the energy and momentum dependence of the resulting QPI signal. Our results also apply to PuB_6 , a strongly correlated topological insulator with a very similar electronic structure.

DOI: [10.1103/PhysRevB.90.201106](https://doi.org/10.1103/PhysRevB.90.201106)

PACS number(s): 71.27.+a, 75.20.Hr, 73.20.At, 03.65.Vf

Topological insulators (TIs) with strong correlations are considered to be of crucial importance in the exciting field of topological phases: They may provide TI states which are truly bulk insulating—a property not easily realized in current Bi-based TIs—and they may host novel and yet unexplored interaction-driven phenomena.

In this context, the material SmB_6 has attracted enormous attention recently, as it has been proposed [1–3] to realize a three-dimensional (3D) topological Kondo insulator (TKI), i.e., a material where f -electron local moments form at intermediate temperatures T and are subsequently screened at low T , such that a topologically nontrivial band structure emerges from Kondo screening [4].

While a number of experiments on SmB_6 , such as transport studies [5–7], quantum oscillation measurements [8], angle-resolved photoemission spectroscopy (ARPES) [9–13], and scanning tunneling spectroscopy (STS) [14,15], appear consistent with the presence of Dirac-like surface states expected in a TKI, a direct proof of their topological nature has been lacking until recently. Moreover, doubts have been raised about the proper interpretation of ARPES data [16,17].

Two types of experiments are usually considered as smoking-gun probes of TI surface states: (i) spin-resolved ARPES which can detect the spin-momentum locking of the surface states [18–20] and (ii) Fourier-transform STS (FT-STs) which can detect the absence of backscattering [18] in quasiparticle interference (QPI) patterns which is a direct consequence of the spin-momentum locking [21–24]. Very recently, spin-resolved ARPES has successfully been applied to SmB_6 and has confirmed spin-momentum locking of the surface states [25]. In contrast, to date no high-quality FT-STs data exist on SmB_6 as well as on other candidate TKI materials, such as PuB_6 [26].

It is the purpose of this Rapid Communication to provide concrete predictions for FT-STs measurements on cubic TKIs. To this end we study the physics of local defects in a multiband Anderson lattice model for SmB_6 and PuB_6 , whose tight-binding (TB) part is derived from band-structure calculations. We determine the spin structure of the three surface Dirac cones and discuss the momentum dependence of the resulting QPI signal for different types of scatterers. Our results may be directly tested in future FT-STs experiments on SmB_6 and PuB_6 .

Multiorbital Anderson model. To describe the electronic properties of both SmB_6 and PuB_6 , which possess the same CsCl-like lattice structure [Fig. 1(a)] and a very similar band structure, we employ a generalized version of the TB model of Refs. [1,3]. The model entails a total of ten rare-earth orbitals per site, namely, the spin-degenerate E_g ($d_{x^2-y^2}$ and d_{z^2}) quadruplet and the lowest-lying f -shell $J = 5/2$ multiplet [see Figs. 1(c) and 1(d)]. Other orbitals, including the rare-earth $J = 7/2$ multiplet and all B_6 states, are excluded, since *ab initio* methods show that their energies are far away from the Fermi level [2,26,27]. The cubic crystal field splits the $J = 5/2$ multiplet into a Γ_8 quadruplet and a Γ_7 doublet, which read $|\Gamma_8^{(1)}\pm\rangle = \sqrt{\frac{5}{6}}|\pm\frac{5}{2}\rangle + \sqrt{\frac{1}{6}}|\mp\frac{3}{2}\rangle$, $|\Gamma_8^{(2)}\pm\rangle = |\pm\frac{1}{2}\rangle$, $|\Gamma_7\pm\rangle = \sqrt{\frac{1}{6}}|\pm\frac{5}{2}\rangle - \sqrt{\frac{5}{6}}|\mp\frac{3}{2}\rangle$, where \pm denotes the pseudospin index.

The total Anderson Hamiltonian is

$$H_0 = H_{dd} + H_{df} + H_{ff} + H_U, \quad (1)$$

with H_U encoding the local interaction and

$$\begin{aligned} H_{dd} &= \sum_{i\sigma\alpha} \epsilon_\alpha^d d_{i\sigma\alpha}^\dagger d_{i\sigma\alpha} - \sum_{\langle ij \rangle \sigma \alpha \alpha'} t_{ij\sigma\alpha\alpha'}^d (d_{i\sigma\alpha}^\dagger d_{j\sigma\alpha'} + \text{H.c.}), \\ H_{ff} &= \sum_{i\sigma\alpha} \epsilon_\alpha^f f_{i\sigma\alpha}^\dagger f_{i\sigma\alpha} - \sum_{\langle ij \rangle \sigma \sigma' \alpha \alpha'} (t_{ij\sigma\sigma'\alpha\alpha'}^f f_{i\sigma\alpha}^\dagger f_{j\sigma'\alpha'} + \text{H.c.}), \\ H_{df} &= \sum_{\langle ij \rangle \sigma \sigma' \alpha \alpha'} (V_{ij\sigma\sigma'\alpha\alpha'} d_{i\sigma\alpha}^\dagger f_{j\sigma'\alpha'} + \text{H.c.}) \end{aligned} \quad (2)$$

being the d and f kinetic energies and the hybridization, respectively. Here, σ and α denote the (pseudo)spin and orbital degrees of freedom, so in the d shell $\sigma = \uparrow, \downarrow$ and $\alpha = d_{z^2}, d_{x^2-y^2}$, while in the f shell $\sigma = +, -$ and $\alpha = \Gamma_8^{(1)}, \Gamma_8^{(2)}, \Gamma_7$.

Hopping and hybridization terms in $\langle ij \rangle$ are included up to seventh nearest neighbor (NN) sites, with $|\mathbf{r}_i - \mathbf{r}_j| \leq \sqrt{9}$. All parameter values were taken from the *ab initio* calculations of Ref. [26], obtained by projecting local density approximation (LDA) results to maximally localized Wannier functions. While these calculations are for PuB_6 , our results should also apply to SmB_6 —perhaps with an adjustment of the overall energy scale (see below)—given the strong similarities of the two materials [26,28]. The concrete values of t_{ij} and V_{ij} up to second NN are given in the Supplemental Material [29].

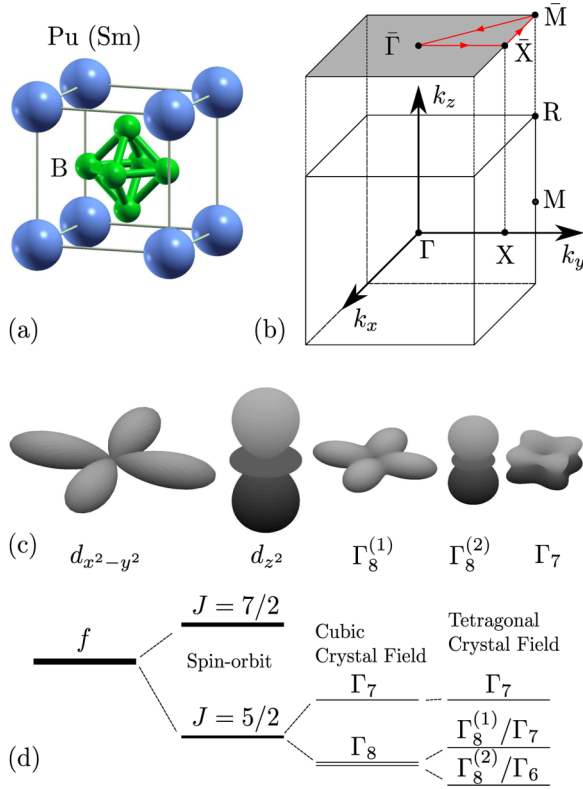


FIG. 1. (Color online) (a) Cubic crystal structure of SmB_6 and PuB_6 . (b) 3D Brillouin zone and its projection to a 2D Brillouin zone for a (001) surface. (c) The five orbitals used in the TB model (all of them Kramers degenerate). (d) Schematic evolution of the f levels under spin-orbit and crystal-field interactions. The tetragonal splitting is relevant near a surface.

Hubbard repulsion and slave-boson approximation. The f electrons are subject to a strong Coulomb repulsion H_U . Here we employ the standard slave-boson approximation which implements reduced charge fluctuations in the infinite-repulsion limit at the mean-field level [30–32]. For both SmB_6 and PuB_6 the dominant charge configurations are $d^1 f^5$ and $d^0 f^6$, such that it is convenient to work in a hole representation: The Coulomb repulsion suppresses states with more than one f hole per site. The remaining states of the local f Hilbert space are represented by auxiliary particles, b_i and $\tilde{f}_{i\sigma\alpha}$ for f^6 and f^5 states, respectively. At the mean-field level, $b_i \rightarrow b = \langle b_i \rangle$ is condensed, and a Lagrange multiplier λ is used to impose the required Hilbert-space constraint. Both parameters need to be determined self-consistently, together with the overall chemical potential; technical details can be found in the Supplemental Material [29].

This procedure transforms the Anderson model of Eq. (1) into a noninteracting TB model, with the influence of the Coulomb repulsion encoded in a downward renormalization of the f kinetic energy by a factor b^2 and the hybridization by a factor b . In addition, the f -level energy ϵ_α^f is shifted towards the Fermi level.

STS, defects, and QPI. To calculate the STS signal on a (001) surface, we solve the renormalized TB model in a slab geometry. We ignore a possible surface reconstruction, but

comment on its effects below [note that the unreconstructed (001) surface of SmB_6 is polar [16]].

In order to model QPI, we take into account scattering off isolated defects which we assume to be located in the surface layer. For simplicity, we take pointlike scatterers and neglect the local modifications of the slave-boson parameters [33]. Impurity-induced changes of electron propagators are calculated using a T -matrix formalism, with details given in the Supplemental Material [29].

The output quantity is the Green's function $G_{aa'}(E, \mathbf{r}, \mathbf{r}')$, which depends on the energy E , on the positions \mathbf{r} and \mathbf{r}' , and on the orbital indices $a, a' = 1, \dots, 10$. The local density of states (LDOS) is the (orbital) trace of the imaginary part of the local Green's function, $\rho(E, \mathbf{r}) = -1/\pi \text{Im Tr } \hat{G}(E, \mathbf{r}, \mathbf{r})$. However, the STS signal is not simply proportional to the LDOS, as the tip samples each orbital with a different weight, and interference effects are also present [34–38]. To simulate this process, in the spirit of the *cotunneling* of Ref. [36], we compute $\rho_{\text{STS}}(E, \mathbf{r}) = -1/\pi \text{Im Tr}[\hat{\psi} \hat{G}(E, \mathbf{r}, \mathbf{r}) \hat{\psi}^T]$, where $\hat{\psi}$ is a 4×10 matrix containing the coupling between each of the ten orbitals to each of four assumed tip-electron channels (two spin directions and two orbitals); for details, see the Supplemental Material [29]. The QPI signal $\rho_{\text{QPI}}(E, k_x, k_y, z = 1)$ is then obtained from $\rho_{\text{STS}}(E, x, y, z = 1)$ by a Fourier transform in the xy plane; ρ_{QPI} is real for the single-impurity case considered here.

Results: Band structure and surface states. Figure 2(a) shows the three-dimensional (3D) band structure as obtained from the renormalized TB model. The d band has a minimum at about -1.7 eV at the X point, as observed in ARPES experiments for SmB_6 [9–13], while f states lie close to the Fermi level

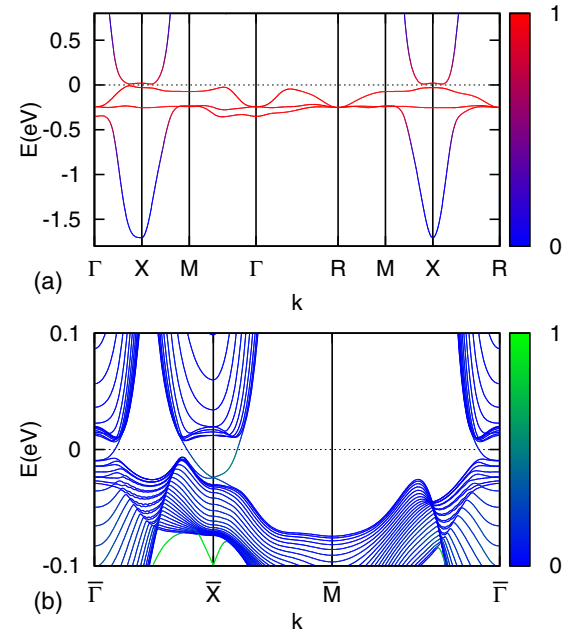


FIG. 2. (Color online) (a) Bulk dispersion from the renormalized TB model along a path in the 3D Brillouin zone; the color code shows the f weight. (b) Band structure of a $n_z = 25$ slab along a path in the 2D (surface) Brillouin zone; the color code shows the spectral weight in the topmost ($z = 1$) layer.

energy. Around the X point, the bottom of the conduction (top of the valence) band is mainly of Γ_7 (Γ_8) character. The overall agreement with DFT calculations, possibly with many-body corrections [2,26,27], is satisfactory, even though reproducing some finer details would require including even longer-range hoppings; we have verified that this does not significantly alter surface states and QPI spectra. We note that, according to dynamical mean-field theory (DMFT) calculations [26], the interaction-induced renormalization factor of the f kinetic energy should be ~ 0.2 rather than our $b^2 \sim 0.5$. Furthermore, LDA results indicate that that f -band energies are by a factor of 1.5–2 smaller in SmB_6 as compared to PuB_6 [2,26]. As a consequence, a rescaling of the bulk energies close to the Fermi level by a factor ~ 0.2 – 0.4 might be necessary for a quantitative comparison with SmB_6 experiments. We stress, however, that this does not strongly affect the *momentum* dependence of the QPI spectra to be discussed below.

By computing topological indices [18,39,40] it is easy to show that the renormalized TB model is a strong topological insulator for the range of parameters pertinent to SmB_6 [1–3] and PuB_6 [26]. Band inversion between even d and odd f bands occurs at the three inequivalent X points. As a result, three surface Dirac cones appear at the two \bar{X} points and at $\bar{\Gamma}$ of the two-dimensional (2D) surface Brillouin zone [1–3,26] [see Fig. 2(b)]. We obtain the Dirac energies to be $\epsilon_{F\bar{\Gamma}} = -9$ meV and $\epsilon_{F\bar{X}} = -24$ meV and the Fermi momenta $k_{F\bar{\Gamma}} = 0.15 \text{ \AA}^{-1}$ and $k_{F\bar{X}} = 0.19$ – 0.17 \AA^{-1} (we have used the SmB_6 lattice constant 4.13 \AA). Experimental results from ARPES for SmB_6 are [9,11,13] $\epsilon_{F\bar{\Gamma}} = -23$ meV, $\epsilon_{F\bar{X}} = -65$ meV, $k_{F\bar{\Gamma}} = 0.09 \text{ \AA}^{-1}$, $k_{F\bar{X}} = 0.39$ – 0.28 \AA^{-1} . While this agreement does not appear perfect, we note that the experimental estimates for $\epsilon_{F\bar{\Gamma}}$ and $\epsilon_{F\bar{X}}$ were obtained by a linear extrapolation of the low- E dispersion [11]; the curvature in our surface bands indicates that this might be unwarranted. In addition, the precise dispersion of surface states sensitively depends on many factors which are difficult to take into account in a microscopic model. These include modified orbital energies, a modified crystal field, and modified Kondo screening [33] near the surface as well as surface termination, surface reconstruction, and disorder. In particular, the unreconstructed (001) surface of SmB_6 is polar, showing also surface states of nontopological origin, while the 2×1 reconstructed surface is nonpolar [14,15], and is the one which more closely resembles our modeling (ignoring reconstruction effects such as band folding [10]). The dependence of in-gap states on the surface termination has also been noted in *ab initio* calculations [41].

Results: STS signal. The energy-dependent STS signal [Fig. 3(a)] shows a pseudogap close to the Fermi energy; at negative (positive) energies the signal originates mainly from f (d) states. Existing STS experiments on 2×1 reconstructed (001) SmB_6 surfaces [14,15] show a peak at roughly -8 meV and a dip near E_F , leading to a Fano-like structure. Its shape and peak-to-background ratio are very similar similar to that in our calculation. However, our peak lies considerably deeper in energy, at about -80 meV, corresponding to a set of surface states, while at about -30 meV, where bulk f states show an LDOS peak, we see no peak in the surface signal. As noted above, surface states are extremely sensitive to the local environment, and changes in their dispersion will strongly influence the STS signal: For example, the

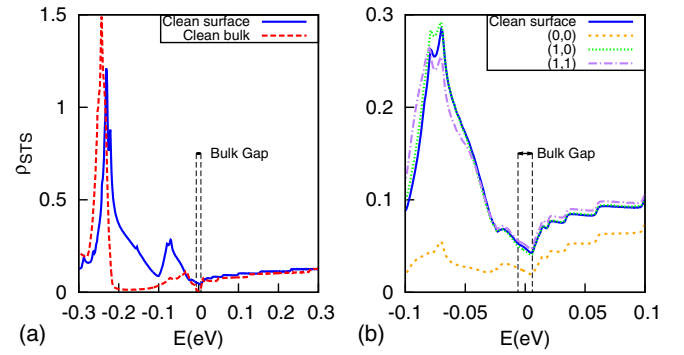


FIG. 3. (Color online) (a) STS signal of a clean surface, together with the hypothetical signal from the bulk obtained by using periodic boundary conditions along z . The residual bulk signal inside the gap, between -6 and 6 meV, arises from the finite Lorentzian broadening used in the calculation. The bulk signal's large peak around -0.3 eV originates from weakly dispersing f states [Fig. 2(a)]. (b) STS signal over a Kondo hole located at $(0,0)$ and in its proximity at $(1,0)$ and $(1,1)$, compared to the signal of the clean surface as in (a).

unreconstructed (polar) surface of SmB_6 displays a peak at -28 meV (instead of -8 meV), and disordered surfaces show even more complex behavior [15]. As a consequence, we believe the peaks observed in experiments at -8 or -28 meV arise from surface (rather than bulk) states, and apparently require a more accurate modeling of states far from the Dirac points.

Near a Kondo hole, i.e., a defect with a missing f orbital, the tunneling spectrum is mainly suppressed at negative energies where the signal has an f character [Fig. 3(b)]. No resonance peaks occur for these strong scatterers, due to the large particle-hole asymmetry of the f band [33]. We note that low-energy resonances may still occur for scatterers of fine-tuned intermediate strength.

Results: QPI signal. In Fig. 4 we show the QPI signal inside the bulk gap for different types of impurities, with the corresponding surface ARPES signal for comparison; the figure also indicates the spin polarization of the surface states [29]. Notably, this spin structure agrees with the recent results of spin-resolved ARPES on SmB_6 [25].

As is common for all TIs, the QPI signal from intracone scattering due to nonmagnetic impurities is weak and nonpeaked near the Dirac point [19,20,42], as backscattering $\mathbf{k} \leftrightarrow -\mathbf{k}$ involves states with opposite spin. No such argument holds for intercone scattering, which, consequently, can give rise to pronounced peaks in the QPI signal [33]. Remarkably, the Dirac-cone spin structure of Fig. 4(b) is such that *also* intercone scattering tends to be suppressed: This is because the spin directions for pairs of stationary points [43] [i.e., points with parallel tangents to their constant-energy contour, e.g., the ones connected by colored arrows in Figs. 4(a)–4(c)] are essentially antiparallel, which applies both to $\bar{\Gamma} - \bar{X}$ and $\bar{X} - \bar{X}'$ scattering [44]. However, care is required: While QPI spectra associated with Γ_8 impurities are mostly nonpeaked [Figs. 4(j)–4(l)], as suggested by the spin structure, both Γ_7 impurities and Kondo holes do give rise to QPI peaks corresponding to $\bar{X} - \bar{X}'$ scattering [see Figs. 4(d)–4(i)]. As

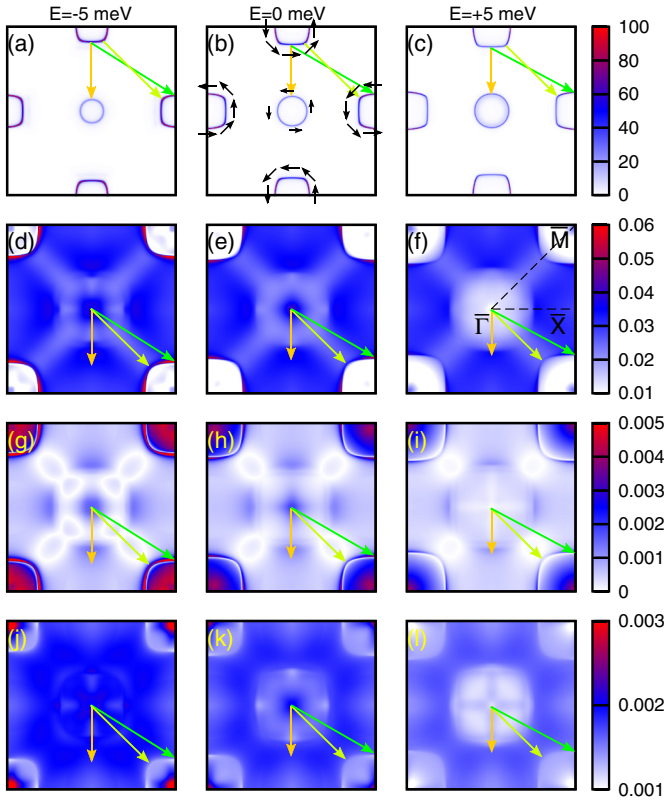


FIG. 4. (Color online) (a)–(c) ARPES signal at -5 , 0 , and $+5$ meV, and corresponding QPI signal $|\rho_{\text{QPI}}|$ for (d)–(f) a Kondo hole, (g)–(i) a weak Γ_7 scatterer, and (j)–(l) a weak Γ_8 scatterer, both in the Born approximation with $V = 10$ meV. In (b) we schematically show the surface-state spin structure [29], which agrees with the experimental results of Ref. [25].

shown in the Supplemental Material [29], this can be ascribed to the Γ_7 component of the surface states which in fact displays parallel spin expectation values at certain pairs of stationary points, allowing for efficient $\bar{X} - \bar{X}'$ scattering. Thus, details of the intercone signal depend on the character of the scattering center, which might help to experimentally identify different scatterers.

The energy dependence of the QPI signal within the bulk gap is weak: Upon increasing the energy, the intercone scattering momenta shrink, and the overall signal strength decreases. Upon leaving the bulk gap, we expect a rapid decrease of the surface QPI signal, due to the hybridization of surface with bulk states.

To underline how sensitively the QPI signal depends on proper modeling, in particular, on the Dirac-cone spin structure, we have repeated the same calculation with models of reduced f -orbital content, i.e., retaining only the Γ_7 doublet or only the Γ_8 quartet in the model Hamiltonian (1), as in Fig. 5 of Ref. [26]. The resulting QPI patterns drastically differ, and the “only Γ_7 ” case even yields a spin structure in disagreement with experiment [25]. Details are in the Supplemental Material [29].

These results show that the orbital content of both surface states and impurities is relevant to QPI spectra. Importantly, this cannot be properly captured in effective low-energy models. In particular, the relative Γ_7/Γ_8 weight of both the Dirac-cone states and the impurities determine the strength of the $\bar{X} - \bar{X}'$ scattering peak of experimental QPI spectra. We note that none of the calculations showed a significant QPI signal for scattering between the $\bar{\Gamma}$ and \bar{X} cones.

Summary. We have computed ARPES, STS, and QPI spectra within a renormalized multiorbital TB model for the strongly correlated TI materials SmB_6 and PuB_6 . Both ARPES and STS spectra agree semiquantitatively with existing experimental results for SmB_6 . The remaining disagreement can be attributed to modeling uncertainties concerning the interaction-induced renormalization of the kinetic energy and the detailed electronic structure of the surface, where surface termination and reconstruction play an important role.

We have made concrete predictions for the QPI signal. We have found that QPI peaks corresponding to $\bar{X} - \bar{X}'$ intercone scattering can appear for particular types of impurities, which can be related to the spin structure and orbital content of the Dirac-cone states. We have also considered a model variant which results in a spin structure in disagreement with experiment [25] and yields a qualitatively different QPI signal, illustrating that QPI is a powerful probe for the surface spin structure of TIs with multiple Dirac cones. Hence, the observation of a weakly peaked low-energy QPI signal in SmB_6 , possibly with $\bar{X} - \bar{X}'$ scattering peaks, would not only confirm the topological nature of the surface states, but also the Dirac-cone spin structure as reported in Ref. [25].

Future work should include a more detailed modeling of surface effects as well as a study of finite-temperature crossovers, similar to Refs. [45,46].

Acknowledgments. We thank H. Fehske, L. Fritz, D. K. Morr, and J. E. Hoffman for discussions and collaborations on related work. Furthermore, we are very grateful to X. Deng, K. Haule, and G. Kotliar for sharing their data on PuB_6 . This research was supported by the DFG through FOR 960 and GRK 1621 as well as by the Helmholtz association through VI-521.

- [1] T. Takimoto, *J. Phys. Soc. Jpn.* **80**, 123710 (2011).
- [2] F. Lu, J. Z. Zhao, H. Weng, Z. Fang, and X. Dai, *Phys. Rev. Lett.* **110**, 096401 (2013).
- [3] V. Alexandrov, M. Dzero, and P. Coleman, *Phys. Rev. Lett.* **111**, 226403 (2013).
- [4] M. Dzero, K. Sun, V. Galitski, and P. Coleman, *Phys. Rev. Lett.* **104**, 106408 (2010).

- [5] S. Wolgast, C. Kurdak, K. Sun, J. W. Allen, D.-J. Kim, and Z. Fisk, *Phys. Rev. B* **88**, 180405(R) (2013).
- [6] D. J. Kim, J. Xia, and Z. Fisk, *Nat. Mater.* **13**, 466 (2014).
- [7] X. Zhang, N. P. Butch, P. Syers, S. Ziemak, R. L. Greene, and J. Paglione, *Phys. Rev. X* **3**, 011011 (2013).
- [8] G. Li, Z. Xiang, F. Yu, T. Asaba, B. Lawson, P. Cai, C. Tinsman, A. Berkley, S. Wolgast, Y. S. Eo, D.-J. Kim, C. Kurdak,

- J. W. Allen, K. Sun, X. H. Chen, Y. Y. Wang, Z. Fisk, and L. Li, [arXiv:1306.5221](https://arxiv.org/abs/1306.5221).
- [9] M. Neupane, N. Alidoust, S. Xu, T. Kondo, Y. Ishida, D.-J. Kim, C. Liu, I. Belopolski, Y. Jo, T.-R. Chang, H.-T. Jeng, T. Durakiewicz, L. Balicas, H. Lin, A. Bansil, S. Shin, Z. Fisk, and M. Z. Hasan, *Nat. Commun.* **4**, 2991 (2013).
- [10] N. Xu, X. Shi, P. K. Biswas, C. E. Matt, R. S. Dhaka, Y. Huang, N. C. Plumb, M. Radovic, J. H. Dil, E. Pomjakushina, K. Conder, A. Amato, Z. Salman, D. M. Paul, J. Mesot, H. Ding, and M. Shi, *Phys. Rev. B* **88**, 121102 (2013).
- [11] J. Jiang, S. Li, T. Zhang, Z. Sun, F. Chen, Z. R. Ye, M. Xu, Q. Q. Ge, S. Y. Tan, X. H. Niu, M. Xia, B. P. Xie, Y. F. Li, X. H. Chen, H. H. Wen, and D. L. Feng, *Nat. Commun.* **4**, 3010 (2013).
- [12] C.-H. Min, P. Lutz, S. Fiedler, B. Y. Kang, B. K. Cho, H.-D. Kim, H. Bentmann, and F. Reinert, *Phys. Rev. Lett.* **112**, 226402 (2014).
- [13] J. D. Denlinger, J. W. Allen, J.-S. Kang, K. Sun, B.-I. Min, D.-J. Kim, and Z. Fisk, [arXiv:1312.6636](https://arxiv.org/abs/1312.6636).
- [14] S. Rößler, T.-H. Jang, D.-J. Kim, L. H. Tjeng, Z. Fisk, F. Steglich, and S. Wirth, *Proc. Natl. Acad. Sci. USA* **111**, 4798 (2014).
- [15] M. M. Yee, Y. He, A. Soumyanarayanan, D.-J. Kim, Z. Fisk, and J. E. Hoffman, [arXiv:1308.1085](https://arxiv.org/abs/1308.1085).
- [16] Z.-H. Zhu, A. Nicolaou, G. Levy, N. P. Butch, P. Syers, X. F. Wang, J. Paglione, G. A. Sawatzky, I. S. Elfimov, and A. Damascelli, *Phys. Rev. Lett.* **111**, 216402 (2013).
- [17] E. Frantzeskakis, N. de Jong, B. Zwartsenberg, Y. K. Huang, Y. Pan, X. Zhang, J. X. Zhang, F. X. Zhang, L. H. Bao, O. Tegus, A. Varykhalov, A. de Visser, and M. S. Golden, *Phys. Rev. X* **3**, 041024 (2013).
- [18] L. Fu, C. L. Kane, and E. J. Mele, *Phys. Rev. Lett.* **98**, 106803 (2007).
- [19] M. Z. Hasan and C. L. Kane, *Rev. Mod. Phys.* **82**, 3045 (2010).
- [20] X.-L. Qi and S.-C. Zhang, *Rev. Mod. Phys.* **83**, 1057 (2011).
- [21] P. Roushan, J. Seo, C. V. Parker, Y. S. Hor, D. Hsieh, D. Qian, A. Richardella, and M. Z. Hasan, *Nature (London)* **460**, 1106 (2009).
- [22] Z. Alpichshev, J. G. Analytis, J.-H. Chu, I. R. Fisher, Y. L. Chen, Z. X. Shen, A. Fang, and A. Kapitulnik, *Phys. Rev. Lett.* **104**, 016401 (2010).
- [23] T. Zhang, P. Cheng, X. Chen, J.-F. Jia, X. Ma, K. He, L. Wang, H. Zhang, X. Dai, Z. Fang, X. Xie, and Q.-K. Xue, *Phys. Rev. Lett.* **103**, 266803 (2009).
- [24] Y. Xia, D. Qian, D. Hsieh, L. Wray, A. Pal, H. Lin, and A. Bansil, *Nat. Phys.* **5**, 398 (2009).
- [25] N. Xu, P. K. Biswas, J. H. Dil, R. S. Dhaka, G. Landolt, S. Muff, C. E. Matt, X. Shi, N. C. Plumb, M. Radović, E. Pomjakushina, K. Conder, A. Amato, S. Borisenko, R. Yu, H.-M. Weng, Z. Fang, X. Dai, J. Mesot, H. Ding, and M. Shi, *Nat. Commun.* **5**, 4566 (2014).
- [26] X. Deng, K. Haule, and G. Kotliar, *Phys. Rev. Lett.* **111**, 176404 (2013).
- [27] C.-J. Kong, J. Kim, K. Kim, J.-S. Kang, J. D. Denlinger, and B. I. Min, [arXiv:1312.5898](https://arxiv.org/abs/1312.5898).
- [28] X. Deng and K. Haule (private communication).
- [29] See Supplemental Material at <http://link.aps.org/supplemental/10.1103/PhysRevB.90.201106> for details about the tight-binding parameters, the slave-boson approach, the scattering matrix technique, the STS signal, the spin expectation value on surface states, and QPI spectra.
- [30] N. Read and D. M. Newns, *J. Phys. C: Solid State Phys.* **16**, 3273 (1983).
- [31] N. Read and D. M. Newns, *J. Phys. C: Solid State Phys.* **16**, L1055 (1983).
- [32] A. C. Hewson, *The Kondo Problem to Heavy Fermions* (Cambridge University Press, Cambridge, UK, 1993).
- [33] P. P. Baruselli and M. Vojta, *Phys. Rev. B* **89**, 205105 (2014).
- [34] V. Madhavan, W. Chen, T. Jamneala, M. F. Crommie, and N. S. Wingreen, *Science* **280**, 567 (1998).
- [35] O. Újsághy, J. Kroha, L. Szunyogh, and A. Zawadowski, *Phys. Rev. Lett.* **85**, 2557 (2000).
- [36] M. Maltseva, M. Dzero and P. Coleman, *Phys. Rev. Lett.* **103**, 206402 (2009).
- [37] J. Figgins and D. K. Morr, *Phys. Rev. Lett.* **104**, 187202 (2010).
- [38] J.-X. Zhu, J.-P. Julien, Y. Dubi, and A. V. Balatsky, *Phys. Rev. Lett.* **108**, 186401 (2012).
- [39] M. Dzero, K. Sun, P. Coleman, and V. Galitski, *Phys. Rev. B* **85**, 045130 (2012).
- [40] L. Fu and C. L. Kane, *Phys. Rev. B* **76**, 045302 (2007).
- [41] J. Kim, K. Kim, C.-J. Kang, S. Kim, H. C. Choi, J.-S. Kang, J. D. Denlinger, and B. I. Min, [arXiv:1405.2511](https://arxiv.org/abs/1405.2511).
- [42] H.-M. Guo and M. Franz, *Phys. Rev. B* **81**, 041102 (2010).
- [43] Q. Liu, X.-L. Qi, and S.-C. Zhang, *Phys. Rev. B* **85**, 125314 (2012).
- [44] Intercone $\bar{X} - \bar{X}'$ scattering does not lead to a strong QPI peak near (π, π) , despite the almost perfect nesting of the two \bar{X} cones: For isotropic cones, intercone scattering by (π, π) is equivalent to intracone scattering by $(0, 0)$, and the latter produces [42] a flat signal near $(0, 0)$ only.
- [45] A. Benlagra, T. Pruschke, and M. Vojta, *Phys. Rev. B* **84**, 195141 (2011).
- [46] J. Werner and F. F. Assaad, *Phys. Rev. B* **89**, 245119 (2014).